ChemCatChem

Research Article
doi.org/10.1002/cctc.202400890

Chemistry Europe
European Chemical Societies Publishing

www.chemcatchem.org

Ammonia Synthesis Rate Over a Wide Operating Range: From Experiments to Validated Kinetic Models

Solmaz Nadiri[+],[a] Alireza Attari Moghaddam[+],[b] Jan Folke,[c] Holger Ruland,[c] Bo Shu,[a] Ravi Fernandes,[a] Robert Schlögl,[c, d] and Ulrike Krewer*[e]

With the increasing demand for flexible operation of ammonia production, the feasibility of using reaction kinetic models to predict the performance of a Haber Bosch reactor in a wide operating range must be evaluated. This study compares the feasibility of a lumped Temkin rate expression with a more complex lumped microkinetic model in predicting turnover rates across diverse temperatures and feed compositions. Evaluation and validation were carried out through ammonia synthesis experiments on a magnetite-based industrial catalyst at temperatures ranging from 548 K to 773 K and H_2:N_2 ratios between 4:1 to 1:1 at 90 bar. While excellent agreement between model predictions and experiments was observed at 648 K, significant discrepancies emerged at 548 K. These findings are valuable for both state-of-the-art ammonia synthesis reactors and green ammonia plants utilizing electrolysis-derived hydrogen, where flexible operating conditions are paramount. Moreover, integrating site density as a function of temperature and the partial pressure of H_2 into the lumped microkinetic model marks a notable advancement, promising enhanced precision in addressing varied operating conditions.

1. Introduction

Reliable prediction of reaction rates is a fundamental element in design, optimization, and performance evaluation of industrial reactors. Industrial ammonia synthesis reactors based on the Haber-Bosch process are operated in a steady state mode at or very close to an optimum operating point. Consequently, reliable rate expressions and advanced reaction kinetics for ammonia synthesis have been validated only within a limited range of industrial operating conditions.

However, in the future, ammonia synthesis reactors may be operated in a wider range of operating conditions, and therefore the rate expressions and kinetic models will need to be valid over a broader range of pressures, temperatures, and compositions. This shift is due to sustainable but intermittent energy resources and CO_2 emission mitigation, as explained below. The Haber-Bosch process is responsible for almost 1% of total energy-related CO_2 emissions, which is mainly due to the use of fossil fuel in its hydrogen production process.[1] As more and more limitations on carbon footprint of chemical processes are implemented through international and local regulations, the Haber-Bosch process must be adapted to comply with such regulations. One practical way to achieve this is through the replacement of the established hydrogen production process from steam reforming of methane with a renewable energy-based process such as water electrolysis; the resulting ammonia synthesis plant would then only be fed by air, water and electricity.[2,3] Such plants may also be downsized and dynamically operated depending on the availability or price of electricity, when replacing the cryogenic air separation with pressure-swing adsorption and adjusting the Haber-Bosch process[3–7] The resulting CO_2-neutral ammonia can not only serve as a chemical but also as a storage medium for renewable energies, where combustion or fuel cells allow for the release of energy.[3,6,7] Alternatives to the Haber-Bosch process focus on electrochemical synthesis of ammonia; yet, whereas significant fundamental research has been dedicated in this area, there is still no technical cell with notable ammonia production.[3,8]

The electrolysis-coupled Haber Bosch process has been recently studied from different technical[9–12] and economical[10,13] aspects. One of the technical challenges of such a process is managing how the synthesis reactor and catalyst can handle the intermittency of renewable resources and thus hydrogen production. If the reactants, hydrogen, and nitrogen, are not stored to guarantee a constant supply to the reactor, such intermittencies will lead to varying operating conditions, especially in composition, inside the synthesis loop.[9,14] This implies that the ammonia synthesis reactor should be operated (dynamically) in a much wider range of operating conditions

[a] S. Nadiri,[+] B. Shu, R. Fernandes
Department of Physical Chemistry, Physikalisch-Technische Bundesanstalt, Bundesallee 100, Braunschweig 38116, Germany

[b] A. Attari Moghaddam[+]
Institute of Energy and Process Systems Engineering, Technische Universität Braunschweig, Braunschweig 38106, Germany

[c] J. Folke, H. Ruland, R. Schlögl
Max Planck Institute for Chemical Energy Conversion, Department Heterogeneous Reactions, Stiftstraße 34–36, 45470 Mülheim an der Ruhr, Germany

[d] R. Schlögl
Fritz Haber Institute of the Max Planck Society, Department of Inorganic Chemistry, Faradayweg 4–6, 14195 Berlin, Germany

[e] U. Krewer
Karlsruhe Institute of Technology, Institute for Applied Materials - Electrochemical Technologies, Adenauerring 20b, 76131 Karlsruhe, Germany
E-mail: Ulrike.krewer@kit.edu

[+] Equally contributing authors.

Supporting information for this article is available on the WWW under https://doi.org/10.1002/cctc.202400890

than the traditional reactors, which differs significantly from the state-of-the-art Haber Bosch process. Cheema et al.[11] demonstrated that off-design operation of typical Haber-Bosch reactor systems is feasible when maintaining auto-thermal operation; the inert gas fraction could be increased by more than 150% of its nominal value or hydrogen intake reduced by 67%, leading to a reduction in ammonia production by 32% or 73%, respectively. High flexibility was also obtained for design variants of reactor systems with regard to the internal heat management.[5] However, H_2 and N_2 streams produced by electrolysis and pressure-swing adsorption contain catalyst poisons like O_2 and H_2O, which strongly deactivate the catalyst even in trace amounts.[14] Also, varied and off-design operation of the reactor can either reversibly or irreversibly affect the activity of the catalyst.[10,14,15] One major point which remains to be assessed is whether the current kinetic rate expressions can give acceptable predictions of the synthesis rate at diverse conditions for a non-deactivated catalyst. Indeed, having an accurate tool for the prediction of the synthesis rate is even more essential for a dynamic process. This would give better operational control and guide operators through an optimum "operating path" over the whole range of operating conditions.

In the traditional Haber Bosch process, nitrogen and hydrogen react over an iron-based catalyst at pressures above 100 bar and temperatures between 673–573 K.[16] The ratio of hydrogen to nitrogen is normally kept close to 3, which is the stoichiometric ratio in the synthesis reaction:

$$N_2(g) + 3H_2(g) \leftrightarrow 2NH_3(g) \quad (1)$$

Argon, present in small amounts (less than 1%), is typically introduced into the reactor as an inert gas. The gas stream also contains trace levels of oxygenates (H_2O, CO, CO_2) and oxygen, which can poison the catalyst reversibly.[14,17] One of the first mathematical expressions for the prediction of ammonia synthesis rate at the commercial conditions of Haber Bosch process was developed by Temkin and Pyzhev in 1940.[18] It assumes that the adsorption of nitrogen on the catalyst surface dominates the rate of ammonia synthesis.[19] Temkin's rate expression is a function of the partial pressures of nitrogen, hydrogen and ammonia and involves a reaction order, α, which is generally between 0.5 and 0.75.[16] A problem with this equation is that the values of reaction order are dependent on temperature, and the rate constants depend on pressure and the H_2:N_2 ratio.[16,20] To improve his rate expression, Temkin incorporated the hydrogenation of the adsorbed nitrogen as the second rate-controlling step and developed a new rate expression in 1963.[21]

Since then, additional modifications have been made to the Temkin equation by different researchers[22–24] Among these, Dyson and Simon[25] used activity instead of partial pressure in the original Temkin rate expression, which led to the elimination of the dependency of rate constants on pressure.[17,25] Dyson and Simon[25] used experimental data from Nielsen et al.[17] under industrial conditions at 149–309 atm, 603–768 K and H_2:N_2 molar ratios between 1.15 and 6.23 to obtain the best fit. They concluded that α values of 0.5 and 0.75 both show a good fit to the measured data. However, the number of data points at nonstoichiometric H_2:N_2 ratios was only a few and therefore the validity of the rate expression at such compositions could not be well assessed. Guacci et al.[24] applied Dyson and Simon's rate expression to? some industrial catalysts at H_2:N_2 ratios of 3 with the values of α ranging from 0.426 to 0.687. Other researchers have used Dyson and Simon's rate expression for the simulation of ammonia synthesis reactors operated close to stoichiometric[26,27] or at non-stoichiometric H_2:N_2 ratios and with changes in inert gas content and temperature.[11,13]

Microkinetic models provide a promising alternative tool for the prediction of the ammonia synthesis rate over a wide range, as they allow for the change of rate-determining steps depending on the operating conditions. The rate expression for ammonia synthesis over iron catalysts obtained from a microkinetic model is based on the concentration of surface species. Stoltze[28] and Bowker[29] developed rate equations based on lumped microkinetic models of ammonia synthesis from surface science studies of single crystals under ultra-high vacuum. In a different approach, Fastrup[30] used temperature programmed adsorption and desorption as well as chemisorption experiments to develop a microkinetic model. Such surface-based models give a detailed insight into the synthesis mechanism, as they describe the catalytic reaction by a network of parallel or serially connected elementary steps that happen at the surface or between the gas phase and surface of the catalyst.

Despite the pressure gap between the ultra-high vacuum experiments and industrial Haber-Bosch reactors, Stoltze's rate equation has proven to give the best predictions for the performance of the industrial iron catalyst over a wide range of operating conditions.[28,31] However, it should be noted that Stoltze strongly reduced the complexity of his model to derive a single rate equation by assuming the dissociation of nitrogen as the rate determining step.[32] To validate his model, Stoltze used industrial data at 150 to 300 atm, N:H ratios of 1:6–1:1 and temperatures of 650–770 K.[17] This was, however, the same set of data that Dyson and Simon[25] used for the validation of their rate expression. As mentioned before, it involves only very few data points at non-stoichiometric H_2:N_2 ratios. Therefore, here too, the predictability of the model could not be fully evaluated at non-stoichiometric compositions. A simplified version of Stoltze's model[33] was validated against ammonia synthesis data over an industrial catalyst at total pressures between 1 and 100 bar and temperatures in the range 593–713 K, while the H_2:N_2 ratio was varied by a factor of 10. The relative standard deviation of the outlet ammonia concentration predicted by the model was relatively high (18%), which may partly be attributed to the simplifications made in the original Stoltze model. Also, the experimental data have not been published, and therefore the discrepancy between simulation and experiment for the data points at off-stoichiometric composition is unknown.

Temkin's rate expression modified by Dyson and Simon as well as Stoltze's model have proven to give reliable predictions of the ammonia synthesis rate over iron-based catalysts at commercial conditions. However, only a few measurements on

industrial catalysts exist at non-stoichiometric composition to assess the predictability of these two kinetic models at such conditions. This is particularly important for the electrolysis-based Haber-Bosch process, where operating conditions may be changed frequently.

Hence, the objective of this study is to conduct supplementary off-design measurements on ammonia kinetics using an industrial catalyst. Additionally, we aim to evaluate the efficacy of Dyson and Simon's and Stoltze's rate expressions in light of these ammonia synthesis measurements across a broad spectrum of temperatures and H_2:N_2 ratios. Furthermore, we provide insights into the intricate surface states obtained from the microkinetic model, assessing the predictability and limitations of both rate expressions. Finally, we extend the lumped microkinetic model by integrating site density as a function of temperature and the partial pressure of H_2, enhancing its predictive capabilities.

The paper is organized as follows: first we will explain the experimental setup and the measurements. After that, Dyson and Simon's and Stoltze's rate expressions are described. This is followed by the results section, where the experimental measurements as well as simulations are presented.

Experimental Method

Ammonia synthesis measurements were conducted in a commercial flow set-up, which includes a guard reactor for feed gas purification, a synthesis reactor containing the catalyst sample with a catalyst bed length of 4.8 cm and a catalyst bed porosity of 87.12%. The dilutant SiC was considered as bed void. The reactor has an inner diameter of 1 cm along with a thermocouple with an outer diameter of 0.3175 cm which is mounted inside the reactor and gives a theoretical reduced reactor diameter of 0.948 cm. The set-up allows measurements at temperatures up to 773 K and a pressure range up to 90 bar. Moreover, the reactor includes an online IR-detector (Emerson X-Stream) for quantitative product gas analysis of NH_3 and H_2O.

To purify the feed gas, i.e., H_2 and N_2 and Ar, from any potential catalyst poisons like O_2 or H_2O, the guard reactor was filled with 150 g of a reduced magnetite-based industrial ammonia synthesis catalyst, which was kept at 313 K during catalytic testing. Before every measurement the guard reactor was regenerated by heating from room temperature at a rate of 1 K/min to 723 K while applying a constant gas flow of 75% H_2 and 25% N_2. The final temperature was kept until the water signal at the reactor outlet was constant. Further information about the set-up can be found in.[34] The temperatures used for controlling the experiments are the temperatures in the catalyst bed.

For the experiments, 1 g of a magnetite-based multipromoted industrial ammonia synthesis catalyst (particle fraction 250–425 μm) was diluted with 1 g of SiC (average particle size 154 μm) and placed in the synthesis reactor. For reduction, the sample was heated at a rate of 1 K/min to 773 K in a gas flow of 440 NmL/min (75% H_2, 25% N_2) at a low pressure of around 3 bar. After reaching 773 K the conditions were kept constant for 18 hours. Subsequently, for catalytic testing, the pressure was increased to 90 bar and the total gas flow was reduced to 200 NmL/min (75% H_2, 25% N_2) while maintaining the temperature at 773 K. These conditions were kept constant for 24 hours to allow further activation of the catalyst due to the increased reductive potential of hydrogen at the higher pressure. A temperature variation was performed by varying the reaction temperatures between 598 and 748 K in 25 K increments, with rates of 1 K/min. Every temperature step was kept constant for 3 hours. The isothermal condition was maintained throughout the experiment by controlling the temperature profiles of the reactor. This was achieved by regulating the temperature using the oven jacket thermocouple, ensuring consistency at temperatures required to maintain 673 or 773 K at the catalyst bed. Following this, the catalyst bed thermocouple was positioned inside the reactor via an immersion tube, incrementally adjusting its location in 1 cm intervals from the uppermost to the lowermost regions of the oven. The resulting temperature profiles, depicted in Figure S1 in the Supplementary Material, reveal the uniform distribution of temperatures within the reactor.

For the partial pressure variation, the total pressure was kept at 90 bar and the total flow rate was increased to 300 NmL/min. The gas composition of the feed gas was altered for the partial pressure of H_2 (P_{H2}) variation from 80 mol-% H_2, 20 mol-% N_2 to 20 mol-% H_2, 20 mol-% N_2, and 60 mol-% Ar by gradually reducing the H_2 content by 10 mol-% and compensation with Ar, covering a H_2:N_2 ratio range of from 4:1 to 1:1. In a similar way the partial pressure of N_2 (P_{N2}) was varied by using the compositions 60 mol-% H_2, 15 mol-% N_2, 25 mol-% Ar; 60 mol-% H_2, 20 mol-% N_2, 20 mol-% Ar and 60 mol-% H_2, 25 mol-% N_2, 15 mol-% Ar covering a H_2:N_2 ratio range of from 4:1 to 2:1. The synthesis rate with these gas compositions was tested at 548, 598 and 648 K. The experimental measurements are summarized in Table S2.

The standard deviation of reproduction measurements was used to calculate the uncertainty of each experiment. The experiments from numbers 1 to 8 were repeated four times under identical conditions (75 mol-% H_2, 25 mol-% N_2, 90 bar, 598–773 K). Table S2 shows the relative standard deviation for these 8 experiments, where the maximum error was 3.2%.

2. Kinetic Models for Ammonia Synthesis

2.1. Stoltze's Lumped Microkinetic Model

According to the microkinetic ammonia synthesis mechanism on a promoted iron catalyst introduced by Stoltze,[28] nitrogen and hydrogen undergo the following elementary steps to produce ammonia:

$$N_2(g) + * \underset{k_{1f}}{\overset{k_{1b}}{\rightleftharpoons}} N_2^* < \mathrm{ZS} > \quad (2.1)$$

$$N_2^* + * \underset{k_{2f}}{\overset{k_{2b}}{\rightleftharpoons}} 2N^* \quad (2.2)$$

$$N^* + H^* \underset{k_{3f}}{\overset{k_{3b}}{\rightleftharpoons}} NH^* + * \quad (2.3)$$

$$NH^* + H^* \underset{k_{4f}}{\overset{k_{4b}}{\rightleftharpoons}} NH_2^* + * \quad (2.4)$$

$$NH_2^* + H^* \underset{k_{5f}}{\overset{k_{5b}}{\rightleftharpoons}} NH_3^* + * \quad (2.5)$$

$$NH_3^* \underset{k_{6f}}{\overset{k_{6b}}{\rightleftharpoons}} NH_3(g) + {}^* \tag{2.6}$$

$$H_2(g) + 2^* \underset{k_{7f}}{\overset{k_{7b}}{\rightleftharpoons}} 2H^* \tag{2.7}$$

where *, k_{jf} and k_{jb} are the free active site on the catalyst surface, and the forward and backward rate constants for reaction step j, respectively. The active site of the catalyst in ammonia synthesis, which is more reactive than the bulk iron atoms, is due to the interaction between the iron sites on the surface and the reactant molecules. Adsorbed species on the surface are denoted by *. Poisoning by oxygen or oxygenates is neglected here and addressed elsewhere.[14] Stoltze's micro-kinetic model assumes that N_2 dissociation is the rate-determining step, and all other reactions are in quasi-equilibrium:

$$K_1 = \frac{k_{1f}}{k_{1b}} = \theta_{N_2} / \left(p_{N_2} \theta*\right) \tag{3}$$

$$K_3 = \frac{k_{3f}}{k_{3b}} = \theta_{NH} \theta* / (\theta_N \theta_H) \tag{4}$$

$$K_4 = \frac{k_{4f}}{k_{4b}} = \theta_{NH_2} \theta* / (\theta_{NH} \theta_H) \tag{5}$$

$$K_5 = \frac{k_{5f}}{k_{5b}} = \theta_{NH_3} \theta* / \left(\theta_{NH_2} \theta_H\right) \tag{6}$$

$$K_6 = \frac{k_{6f}}{k_{6b}} = p_{NH_3} \theta* / \theta_{NH_3} \tag{7}$$

$$K_7 = \frac{k_{7f}}{k_{7b}} = \theta_H^2 / \left(p_{H_2} \theta_*^2\right) \tag{8}$$

where K_j, θ, and p_n are the equilibrium constant of step j, the surface coverage of adsorbed reactants and intermediates or free sites, and the partial pressure of $n \in \{N_2, NH_3, H_2\}$ in Pa, respectively. The rate constants are calculated using the Arrhenius equation:

$$k = k_0 \exp(-E_a / RT) \tag{9}$$

where k_0, E_a, R and T are the pre-exponential factor, activation energy in kJ/mol, ideal gas constant in J/K.mol and temperature in K, respectively. Using the formal kinetic rate equation for the rate-determining step and knowing that the total concentration of species at the surface is equal to the number of active sites, the ammonia synthesis rate in moles per second can be expressed as:[28]

$$\dot{n}_{out,\ Stoltze} = k_{2f} K_1 \left(p_{N_2} - p_{NH_3}^2 / (K_{eq} p_{H_2}^3)\right) \theta_*^2 \mu_s m_{cat} \tag{10}$$

where μ_s and m_{cat} are active site density in mol/g and the weight of the catalyst in g, respectively. $\theta*$ is the coverage by free sites, which implies the likelihood that a given site is not occupied.

$$\theta* = \left(\begin{array}{l} 1 + K_1 \frac{p_{N_2}}{p_0} + \frac{p_{NH_3} p_0}{K_3 K_4 K_5 K_6 K_7^{1.5} p_{H_2}^{1.5}} + \frac{p_{NH_3}}{K_4 K_5 K_6 K_7 p_{H_2}} \\ \\ + \frac{p_{NH_3}}{K_5 K_6 K_7^{0.5} p_{H_2}^{0.5} p_0^{0.5}} + \frac{p_{NH_3}}{K_6} + K_7 \frac{p_{H_2}^{0.5}}{p_0^{0.5}} + \frac{K_8 p_{H_2O}}{p_{H_2}} \end{array} \right)^{-1.0} \tag{11}$$

K_{eq} is the equilibrium constant of the gas phase and is calculated as:

$$K_{eq} = K_1 K_2 K_3^2 K_4^2 K_5^2 K_6^2 K_7^3 \tag{12}$$

The kinetic parameters for the calculation of the reaction rate based on the lumped microkinetic model (Equation (10)) are taken from[28,31] and are listed in Table 1. m_{cat} is set to the experimental value of 1 g. The site density in Equation (10) is assumed to be the only unknown parameter in our simulations and will be estimated from the experimental measurements.

To simulate the experimental reactor, we assume pure convective axial flow in the fixed bed reactor and neglect thermal effects as well as diffusion-based mass transfer. To evaluate the inherent reaction conditions in the context of ammonia synthesis experiments, the relevant criteria were assessed using the EUROKIN spreadsheet,[35] which is designed for evaluating transport limitations in gas-solid fixed beds. Employing the Stoltze rate of reaction equation (Equation (10)), the criteria for transport limitations were computed, assuming a reaction order for N_2 of 1 (see Equation (10)). Additional details can be found in the Supplementary Material. The results presented in Table S1 demonstrate that all assessed criteria are met, suggesting the absence of mass or heat transfer limitations under the specified experimental conditions and the validity of the transport model. To obtain the outlet ammonia concentration, the catalyst bed was discretized into 10,000 equidistant cells along the axial dimension. This number of cells was proven to be enough to ensure that the results are independent of the numerical discretization. The conversion of nitrogen at computational node i (i changes from 1 to 10,000), is then calculated as:

$$X_{N_2,i} = r_{i-1} / F_{N_2,i-1} \tag{13}$$

Table 1. Equilibrium and rate constants based on Arrhenius equation (Equation (9)).[28,31]

Parameter	k_0	E_a (kJ/mol)
K_1	1.3×10^{-8} bar^{-1}	−43.1
K_2	3.25	−126.5
k_{2f}	4.29×10^{9} s^{-1}	28.5
K_3	159.1	58.1
K_4	9.5	36.4
K_5	1.67	38.7
K_6	20600 bar	39.2
K_7	2.1×10^{-7} bar^{-1}	−93.8

where F_{N2} and r are the molar flow rate of nitrogen and the molar ammonia synthesis rate at node i, respectively. The mole fraction y of gas components at computational nodes is determined by mass conservation. For example, for ammonia we have:

$$y_{NH_3,i} = \frac{y_{NH_3,i-1} + 2X_{N_2,i}\, y_{N_2,i-1}}{1 - 2X_{N_2,i}\, y_{N_2,i-1}} \tag{14}$$

The total molar flow rate of all gas components at node i can then be obtained as:

$$F_i = \frac{F_{N_2,i-1}}{y_{N_2,i}}\left(1 - X_{N_2,i}\right) \tag{15}$$

Knowing the molar flow rates, the nodal partial pressure of each component can be calculated by the ideal gas law. A comparison of volumetric flow rates obtained using the ideal gas law, Peng-Robinson, and Redlich-Kwong equations of state is provided in the supplementary material (Figure S2), validating that the ideal gas law is sufficient.

2.2. Dyson and Simon Equation

Dyson and Simon[25] modified the original Temkin equation for the ammonia synthesis rate in kilomoles of ammonia formed per cubic meter of catalyst bed per hour as follows:

$$\dot{n}_{out,\,Dyson} = 2k\left[K_a^2 a_{N2}\left(\frac{a_{H2}^3}{a_{NH3}^2}\right)^{\alpha} - \left(\frac{a_{NH3}^2}{a_{H2}^3}\right)^{1-\alpha}\right] \tag{16}$$

in which k, α_n, Ka, represent the rate constant, the activity of $n \in \{N_2, H_2, NH_3\}$ and equilibrium constant based on activity, respectively. The definition of the activity and the equilibrium constant is provided in the supplementary material. The rate constant is assumed to follow the Arrhenius equation, Equation (9). The parameters α and the pre-exponential factor as well as the activation energy of the rate constant k are the unknowns of Dyson and Simon's equation and should be estimated from the experimental results.

2.3. Further Calculations

To use both models to predict the produced ammonia under the experimental conditions, a set of data, referred to as training data, was used to fit the unknown parameters of the models. Selecting a proper set of data ensures the better performance of the models. For this measure, efficiency was selected. Efficiency is defined as the ratio of the mole fraction of ammonia at the outlet to the maximum achievable mole fraction (at equilibrium) of ammonia.

The equilibrium mole fractions were calculated based on reaction stoichiometry as follows:

$$K_{eq} = \frac{y_{NH_3}^{2\ eq}}{y_{H_2}^{3\ eq} \cdot y_{N_2}^{\ eq}} p^2 \tag{17}$$

Given the equilibrium constant calculated from Equation (12), all the mole fractions in this formula are assumed to be at equilibrium and can be related to each other through the stoichiometric coefficients and a series of mass balance equations. Finally, the calculated mole fraction of ammonia was employed to calculate the efficiency of each experiment.

2.4. Training Data

The data points with efficiencies between 0.15 and 0.8 were selected as training data. By removing the data with high efficiency (>0.8), we eliminated data and reaction rates that could be strongly affected by equilibrium, resulting in an error when estimating rate constants. Conversely, data with low efficiency correspond to very low ammonia output, where measurement errors may play a significant role in the accuracy of the data. Figure S3 in the supplementary material shows the efficiency of all 44 experiments. As a result, 18 points which are highlighted in red in Table S2, were chosen as training data, whereas the rest of the experimental points in this table were used as test data to evaluate the performance of the models.

3. Results

3.1. Experimental Results

In Figure 1, the results of the effect of temperature variation on ammonia outlet concentration for a constant feed gas composition of 75% H_2 and 25% N_2 are shown. The outlet mole

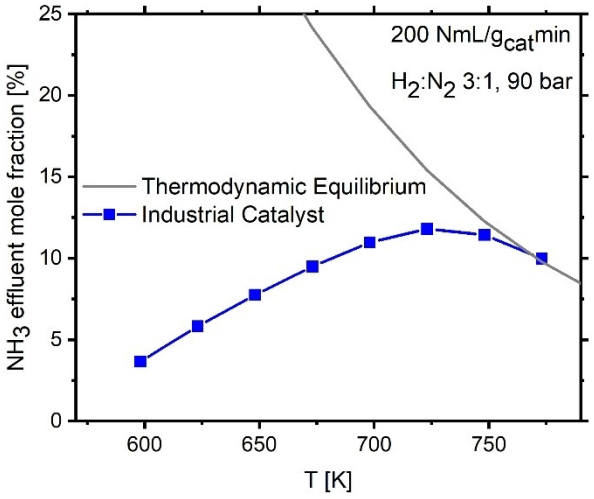

Figure 1. The effluent mole fraction of ammonia in an ammonia synthesis process with a magnetite-based industrial catalyst compared to the thermodynamic equilibrium at 598–773 K and at 90 bar. The equilibrium effluent ammonia fraction was calculated with Aspen Plus software (V10.0).

fraction of NH_3 first increases with rising temperature in a non-exponential manner around 598 K to 698 K; the only small temperature dependence may be caused by product inhibition from the formed ammonia. As ammonia has a negative reaction order[28,36] and a negative influence on the reaction rate at a higher temperature, the conversion only increases slowly and is finally fully limited by the thermodynamic equilibrium, which is reached at 773 K. An 80% efficiency is reached at approximately 723 K.

Figure 2A depicts the variation in ammonia efficiency with increasing temperature across different H_2:N_2 ratios. Experimental data were collected at three distinct temperature levels: 548, 598 and 648 K. Within each temperature category, a range of H_2:N_2 ratios, spanning from 0.93 to 3.8, was explored, encompassing conditions of stoichiometric balance as well as deviations towards hydrogen or nitrogen excess. The experiments involved varying the H_2:N_2 ratio while maintaining a constant mole fraction of N_2 at around 0.21, with the H_2 mole fraction ranging from 0.195 to 0.792.

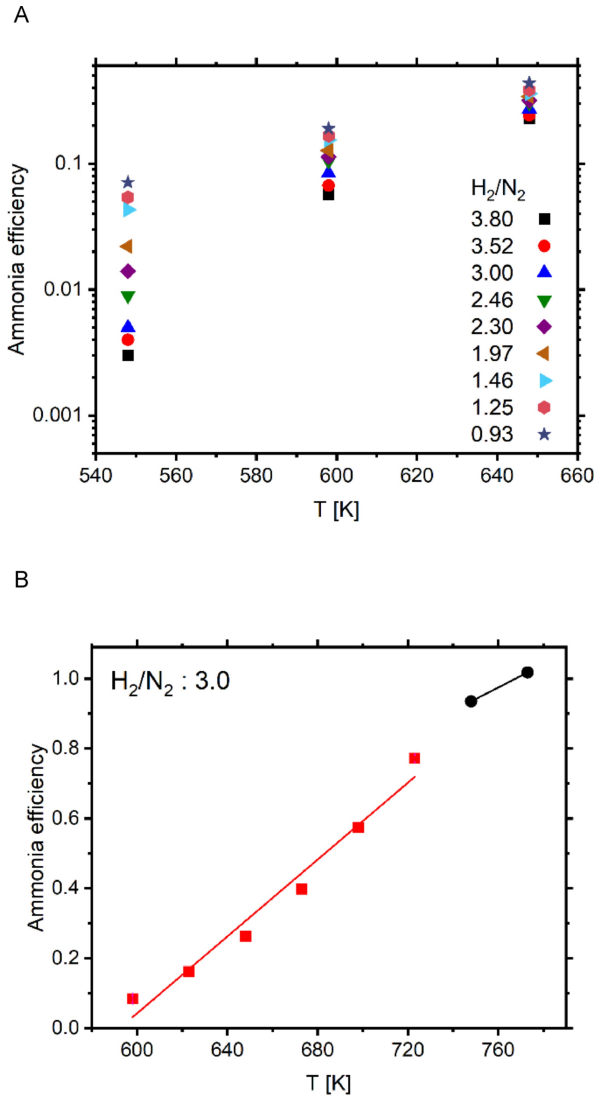

Figure 2. Experimentally observed variation in ammonia efficiency; A) at temperatures of 548, 598 and 648 K and H_2:N_2 ratios of 0.93–3.80, B) at temperatures of 598–773 K and H_2:N_2 ratio of 3.0.

Across all temperatures investigated, it was consistently noted that the highest H_2:N_2 ratio of 3.8 yielded the lowest rates of ammonia synthesis. Conversely, decreasing the H_2:N_2 ratio led to a significant increase in ammonia efficiency. For instance, at 548 K, the ammonia efficiency at an H_2:N_2 ratio of 3.8 was minimal, whereas it rose to nearly 2200% to reach 0.071 at a H_2:N_2 ratio of 0.93. This trend persisted across temperatures, with the efficiency increasing by approximately 400% from 0.057 to 0.19 at 598 K and almost doubling at 648 K.

Figure 2A depicts the variation in ammonia efficiency with increasing temperature across different H_2:N_2 ratios. Experimental data were collected at three distinct temperature levels: 548, 598 and 648 K. Within each temperature category, a range of H_2:N_2 ratios, spanning from 0.93 to 3.8, was explored, encompassing conditions of stoichiometric balance as well as deviations towards hydrogen or nitrogen excess. The experiments involved varying the H_2:N_2 ratio while maintaining a constant mole fraction of N_2 at around 0.21, with the H_2 mole fraction ranging from 0.195 to 0.792.

Across all temperatures investigated, it was consistently noted that the highest H_2:N_2 ratio of 3.8 yielded the lowest rates of ammonia synthesis. Conversely, decreasing the H_2:N_2 ratio led to a significant increase in ammonia efficiency. For instance, at 548 K, the ammonia efficiency at an H_2:N_2 ratio of 3.8 was minimal, whereas it rose to nearly 2200% to reach 0.071 at a H_2:N_2 ratio of 0.93. This trend persisted across temperatures, with the efficiency increasing by approximately 400% from 0.057 to 0.19 at 598 K and almost doubling at 648 K.

At high H_2:N_2 ratios, an excess of hydrogen undermines nitrogen utilization, resulting in diminished ammonia production. This phenomenon arises from the preferential adsorption and consumption of hydrogen on catalytic sites, leaving nitrogen underutilized. Conversely, decreasing the H_2:N_2 ratio enhances nitrogen availability, promoting its participation in ammonia synthesis and a consequent efficiency rise. Variations in H_2:N_2 ratios influence the surface coverage of reactants and intermediates (see section below), modulating the kinetics of ammonia synthesis. Moreover, thermodynamic considerations, including equilibrium shifts and activation energies, contribute to the observed trends, shaping the efficiency-temperature dependence across different stoichiometries.

In the observed trends in ammonia efficiency with varying temperatures and H_2:N_2 ratios, it is essential to consider the nature of active sites on the catalyst surface. Active sites are pivotal regions on the catalyst surface where chemical reactions take place, exerting a profound influence on reaction kinetics and product formation. At 548 K, the observed minimal efficiency of ammonia at higher H_2:N_2 ratios suggests a predominance of weak active sites on the catalyst surface. Weak active sites may exhibit limited binding affinity for reactant molecules and lower catalytic activity compared to moderate or strong active sites. Consequently, under these conditions, the utilization of reactants, particularly nitrogen, may be inefficient, leading to diminished ammonia production.

In contrast, at 598 K and 648 K, where higher efficiencies of ammonia were observed across a range of H_2:N_2 ratios, the active sites likely possess moderate activity. Moderate active sites offer intermediate binding affinity for reactant molecules, facilitating more efficient adsorption and activation compared to weak active sites. Hence, reaction rates and product efficiencies are enhanced, improving ammonia synthesis efficiency.

The iron-nitrogen phase diagram, given by Hansen,[37] highlights notable alterations in the catalyst's phases corresponding to temperature variations. In the lower temperature range, spanning from 300 K to 548 K, Fe_4N dominates as the stable phase, accompanied by a minor presence of Fe_2N. Despite its thermodynamic metastability in nitrogen or inert atmospheres at normal pressure, Fe_4N emerges as the primary phase. Additionally, Fe_2N, though thermally less stable, coexists within the z phase region. With rising temperatures, a shift towards other stable phases occurs. Beyond 548 K, the prevalence of Fe_2N or further formation of Fe_4N suggests a thermodynamically favorable phase progression. These temperature-driven phase transitions reflect dynamic structural alterations within the catalyst, significantly impacting its catalytic behavior and efficiency in ammonia synthesis.[19]

Figure 2B shows the variation of ammonia efficiency with temperature ranging from 598 K to 773 K at a constant H_2:N_2 ratio of 3.0. The slopes of the corresponding line to the experimental points indicate that moderate active sites are valid until the temperature reaches 723 K, beyond which a transition to strong active sites is observed. Strong active sites exhibit enhanced binding affinity and catalytic activity, further boosting reaction rates and product efficiencies. The transition from weak to moderate and eventually strong active sites with increasing temperature reflects temperature-induced changes in catalyst structure and surface properties. At higher temperatures, catalysts may undergo structural modifications or phase transformations, leading to the emergence of more active catalytic sites capable of promoting ammonia synthesis reactions more effectively. The ammonia synthesis rate per mass of catalyst, $\dot{n}_{out}$, is given in Figure 3 for a variation in the partial pressure of hydrogen and nitrogen. The dependence of the synthesis rate on hydrogen partial pressure strongly depends on the temperature; this is related to conversion, as the conversion strongly changes with temperature.

On the other hand, the behavior under nitrogen variation at different temperatures shows a similar progression for all temperatures in the analyzed pressure range. At a low temperature of 548 K, with increasing hydrogen partial pressure up to around 28 bar, the catalytic synthesis rate increases slightly, whereas increasing H_2 partial pressure beyond 28 bar has a negative influence on the synthesis rate. At 598 K, the synthesis rate reaches a maximum at a hydrogen partial pressure of about 55 bar, followed by a slight decrease in synthesis rate with increasing H_2 partial pressure.

At 648 K, in the given pressure range, a sharp increase in catalytic synthesis rate is observed. In contrast, the variation of the nitrogen partial pressure leads to an increasing synthesis rate with increasing nitrogen partial pressure (cf. Figure 3B). At

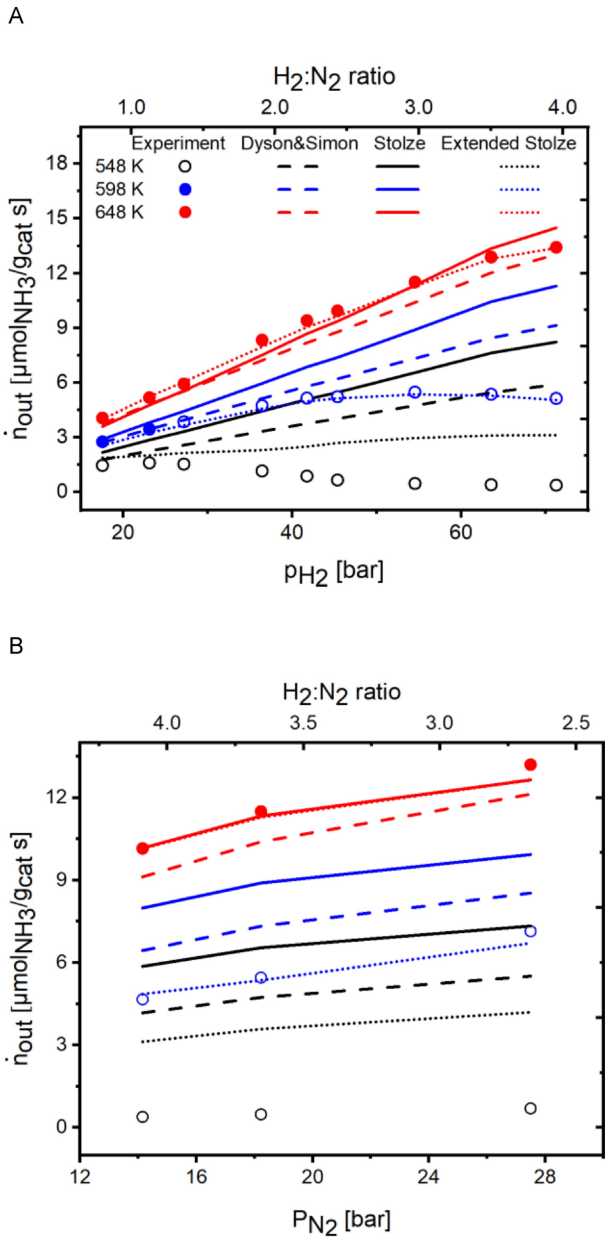

Figure 3. Ammonia synthesis rate per mass of catalyst, $\dot{n}_{out}$, for the magnetite-based industrial catalyst at different temperatures and partial pressures of A) hydrogen (p_{H2}) and B) nitrogen (p_{N2}) at overall pressure of 90 bar. For A, p_{N2} was kept constant at 18 bar and for B, p_{H2} was kept constant at 54 bar. (Symbols: experimental points, with filled circles representing the training data; Lines: predictions by Stolze's rate equation (solid) and Dyson and Simon's rate equation (dashed lines).

higher temperatures, the catalyst synthesis rate rises with a steeper slope, whereas the synthesis rate improvement at 548 K is negligible in the analyzed pressure range. The behavior observed in Figure 3 might be explained by the blocking of the active sites by H_2 for N_2 adsorption at high hydrogen content. Our prior simulation studies with Stolze's model, including poisoning, showed a maximum in synthesis rate with increasing H_2:N_2 ratio; the simulation showed that this was caused by an asymptotic decrease of synthesis rate and N surface coverage

with increasing H content[14] compared to the thermodynamic equilibrium at 598–773 K and at 90 bar.

3.2. Simulation Results

3.2.1. Temkin-Type Kinetic Model

As described previously, Dyson and Simon[25] showed that their slight modification to the Temkin equation improved the predictability of the equation in the calculation of ammonia production rate for the experimental kinetic data from Nielsen et al.[17] Our experimental data obtained at 90 bar were employed to determine k and α in the Dyson and Simon equation by assuming the plug flow model.

By substituting the rate of ammonia production in terms of X_{N2} in Equation (16) and integrating over the length of the catalyst bed (L), k can be determined from the following integral expression:

$$k = \frac{F^{\circ}_{N_2}}{AL}\int_{X=0}^{X=X_{N2e}} \frac{1}{\left[K_a^2 a_{N2}\left(\frac{a_{H2}^3}{a_{NH3}^2}\right)^{\alpha} - \left(\frac{a_{NH3}^2}{a_{H2}^3}\right)^{1-\alpha}\right]} dX_{N_2} \qquad (18)$$

where $X_{N2e}$is the fractional conversion at the exit, and L is the length of the reactor (48 mm). The integral equation was solved numerically for α = 0.25–0.75 with an increment of 0.05. In the literature, α values from 0.5 to 0.75 are reported for industrial catalysts, but our investigation was carried out for a wider range of α to observe the performance of Dyson and Simon's equation at lower α.

Evaluation of Equation (18) at different α was done/conducted using the selected training data from this work. Two data points at a temperature of 598 K were excluded from the experimental points selected in this work to determine the unknown parameter of the Dyson and Simon equation.

This adjustment was necessary because, within the studied range for α, the calculated *k* values at α ≥ 0.7 at 598 K were negative, which is physically infeasible.

The calculated *k* based on the? Equation (18) for α varies? from 0.25 to 0.75, was plotted in an Arrhenius-type plot as a function of 10000/2.303 RT, as shown exemplarily for α = 0.654 in Figure 4. Figure S4 shows the coefficient of determination (R^2) of the linear regression for all α values. The highest value was observed at α = 0.654 with R^2=0.989; at this point, R^2 showed a clear – and the only - maximum. The identified value of α = 0.654 is in agreement with the reaction order obtained by Nielsen et al.[38] for the experimental conditions of 603–773 K and pressures of 150 and 300 atm. Furthermore, the Arrhenius-plot in Figure 4 shows a clear linear behavior, which allowed us to determine k_0 and E_a as $6.5\times10^{+13}$ kmol/(m^3 h) and 159.4 kJ/mol. The obtained activation energy is comparable with the value reported by Dyson and Simon[25] with 7% difference.

The estimated Arrhenius parameters were inserted into Equation (16) to determine the molar fraction of ammonia at the reactor exit at each experimental point. The comparison between the experimental ammonia molar fraction and the

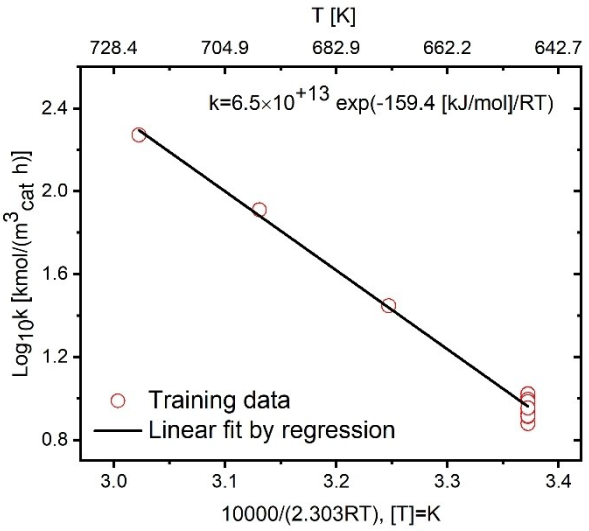

Figure 4. Dependence of identified rate constant k of Dyson and Simon's rate equation on temperature T for α = 0.654.

model-predicted data based on Dyson and Simon's rate equation for α = 0.654 is shown using the parity plot in Figure 5. In this figure, line y = x is used as a reference along with ±10% error lines (dashed lines). When a value from an experimental test equals one from the Dyson and Simon equation, the point will be on the y = x line. As can be seen in Figure 5, the prediction using Dyson and Simon's rate equation for the training data and the test data at temperatures above 623 K is satisfactory, with a maximum discrepancy of 10% at some points. For temperatures at 598 K, a considerable discrepancy can be seen between experiment and simulation, except for five points that lie on the y = x line. A particular focus should be placed on the predictability of Dyson and Simon's rate equation for the two experimental points that were excluded from the

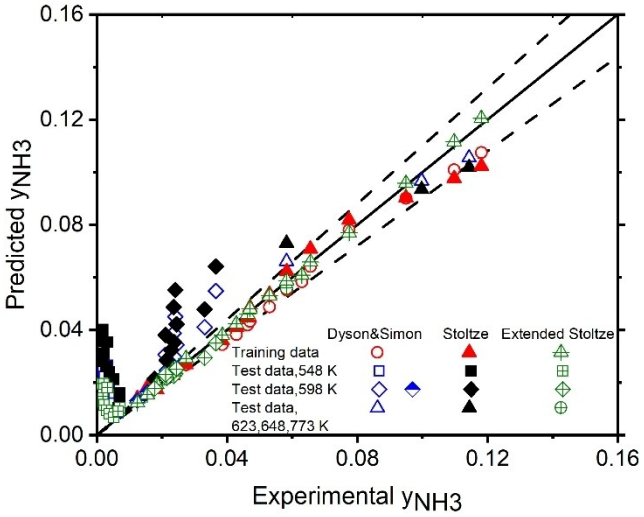

Figure 5. Parity plot showing the predictions of the molar fraction of ammonia at the outlet versus experimental values. The models use either the Temkin-type rate equation of Dyson and Simon or the rate equation of Stoltze. Dashed lines indicate ±10% error intervals.

training data. Dyson and Simon's rate equation is quite accurate in predicting the mole fraction of synthesized ammonia for those two points, symbolized by half-filled blue rhombuses in Figure 5, showing experimental ammonia mole fractions of 0.01547 and 0.01243, with only a 5% deviation/error. It can be concluded that all training data points within the selected efficiency range can be predicted well by the Dyson and Simon equation, and the model's predictability is independent of temperature for the experiments conducted at 598 K, where the H_2:N_2 ratio or the flow rate may affect the model's prediction.

At 548 K, however, the deviation between experiment and model is large, ranging from 30% to 1400% for increasing molar fractions. This confirms literature findings[38] that Dyson and Simon's rate equation, which covers a wide range of high-pressure operating conditions, is not suitable for predicting the rate of ammonia synthesis at temperatures lower than 600 K. A change in mechanism or rate-determining step may be present at such low temperatures.

Moreover, by comparing the calculated rate of ammonia production by Dyson and Simon's equation with the experimental results, this Temkin type rate equation predicts the rate of ammonia for all H_2:N_2 ratios satisfactorily at 648 K for both variants-constant nitrogen pressure (Figure 3A) and constant hydrogen (Figure 3B). Yet, in both cases, a considerable over-prediction can be observed at 598 and 548 K. In Figure 3A, at 598 K, Dyson and Simon's equation indicates that the rate of ammonia production continuously increases as the hydrogen content increases, whereas experimental results indicate that a plateau is reached above an H_2:N_2 ratio of 2.26. The experiment even shows a slight decline in ammonia production at 548 K, forming a plateau at an H_2:N_2 ratio of 3, whereas the model shows a continual rise in ammonia production with an increasing H_2:N_2 ratio. It is possible that the discrepancy between the model and experiment at 598 and 548 K is due to a self-poisoning effect[19,34] that cannot be reproduced by the model.

In contrast, while the model overestimates ammonia production rates at 598 and 548 K, it accurately captures the trend as the N_2 content increases under constant hydrogen flow (Figure 3B).

3.2.2. Model with Stoltze's Rate Equation

In the following, we analyze whether the model based on Stoltze's rate equation (Equation (10)) suits better to reproduce the experimentally observed ammonia synthesis kinetics. As previously mentioned, the only parameter to be identified is the active site density μ_s.

Values of $\mu_s = 20$–30, 60 and 94 μmol/g for the older generation of triply-promoted iron catalyst (industrial) are reported in literature.[33,39,40] Considering possible improvements in recent years of industrial catalyst development, higher active site density might be expected for our catalyst. Thus, a lower- and upper bound of 50 and 150 were considered, respectively, to estimate the site density based on the experimental conditions. The optimization algorithm minimized the absolute difference between the experimentally determined molar fraction of ammonia at the outlet (y_{exp}) and that predicted by the model (y_{model}). As a result, a site density of 125 μmol/g showed the best fit to the experimental data.

The mole fraction of ammonia predicted with Stoltze's rate equation is also plotted in Figure 5 in a parity plot with the experimental data. It can be seen that, similarly to the Temkin-type kinetic model, Stoltze's rate equation reproduces the training data and the test data at high temperatures, but not the experimental data recorded at lower temperatures. Indeed, very similar trends to the Temkin-type kinetic model in terms of deviation from experiment can be seen; the predicted points are very close to each other.

As explained earlier, in the Stoltze kinetics model, the active site density μ_s was only adjusted, whereas in the Temkin-type kinetic model, three parameters (pre-exponential factor, activation energy and α) were fitted to the experimental data. Yet, Equation (10) also has a nonlinear dependence on the equilibrium constant K_{eq}, and numerous temperature-dependent kinetic parameters may have changed compared to the catalyst used for the extraction of kinetic parameters by Stoltze. These points could justify the better predictability of the Temkin-type kinetic model compared to Stoltze's. To determine whether adjusting the kinetic constants would improve the quantitative capability of the model with Stoltze's kinetics in predicting the concentration of produced ammonia, a global optimization method was employed for the kinetic parameters of Stoltze's model. In this method, a constrained multi-objective genetic algorithm approach was used for optimization. The objective function was defined as the difference between the calculated ammonia mole fraction by the microkinetic model and the experimental values. The targeted variables were the pre-exponential factors and activation energy of all reactions. The training data were selected to cover all the temperatures from 548 K to 773 K and all H_2:N_2 ratio. Yet, the additional degree of freedom did not lead to a better reproduction of experiments, as can be seen in Figure S5. Indeed, here too, the progression is very similar to that of the previously analyzed two models, indicating a systematic lack of specific features in the present models at low temperatures.

As illustrated in Figure 3, detailed analysis shows that deviations occur both at low temperatures and at high H_2:N_2 ratios, similar to Dyson and Simon's equation. For industrial applications, and especially for green ammonia production, the range where the models fail is less relevant since the temperature is high (>673 K). The model fails to capture the experiments at all at 548 K and some of the experiments at 598 K with $P_{H2} > 30$ bar. This indicates that the lumped microkinetic approach for ammonia synthesis, which assumes that the rate limiting step is N_2 dissociation and all other steps are fast and thus in equilibrium, is not adequate to account for hydrogen inhibition on the catalyst surface.

Stoltze and co-workers[28] showed experimentally that H_2 inhibition is more significant at low temperatures, low ammonia partial pressure, and high partial pressure of H_2. Although the predictability of Stoltze's rate equation at low temperatures is limited, it still can qualitatively indicate a trend of H_2 inhibition.

H_2 inhibition leads to pushing N* off the surface and therefore reducing the activity.

At higher temperatures, this effect is not as pronounced as at lower temperatures since the hydrogen adsorption is exothermic. However, it could still occur at very high temperatures, as we see at T = 648 K, which is approaching a plateau with increasing P_{H2}. In fact, high surface coverages by H* also occur at low conversion and high P_{H2} (e.g., the inlet of the reactor).

Figure 6 shows the surface coverage of the adsorbed species H* and N*at different partial pressures of hydrogen predicted by the model with Stoltze's kinetics. As can be seen in the figure, the model shows that the coverage of the surface by H* at 548 K is higher than at 598 K and 648 K; but on the other hand, the surface coverage by N* at 548 K is the lowest compared to the higher temperatures. Additionally, the higher partial pressure of H_2 leads to a higher surface coverage by atomic hydrogen. Yet, with the present parameter set, the model does not predict an adequately strong inhibition similar to that observed in the experiment for the analyzed range of high P_{H2}. However, poisoning by oxygen species at low temperatures cannot be ruled out.

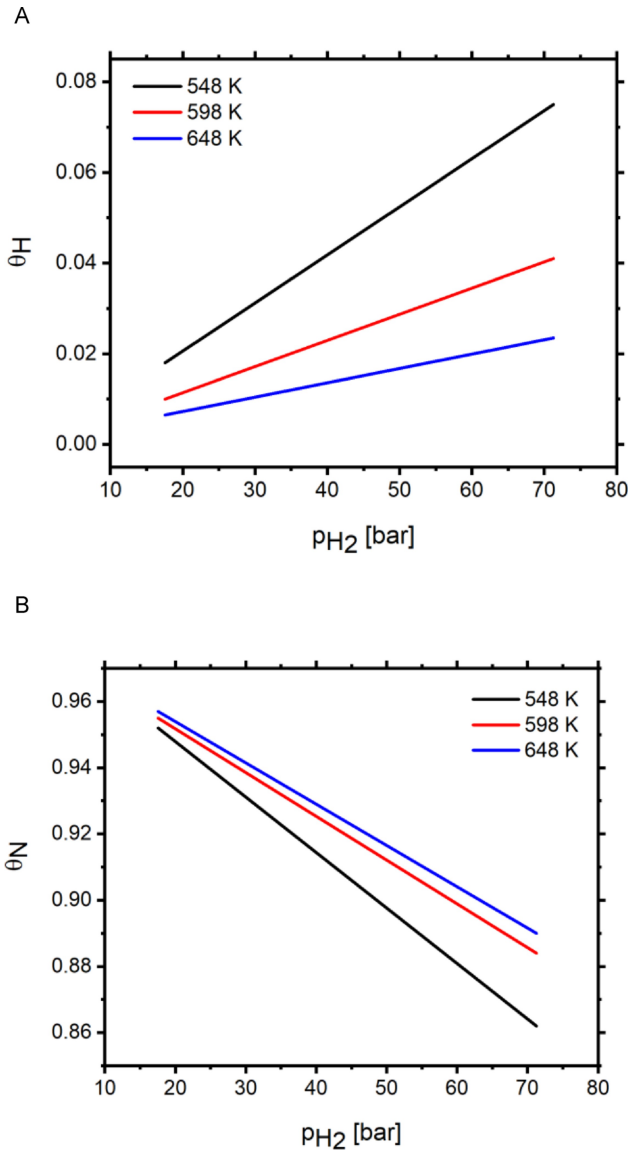

Figure 6. Prediction by the model with Stoltze's rate equation at temperatures of 548, 598 and 648 K, at different partial pressures of hydrogen and a constant N_2 mole fraction of ~0.205, for the surface coverage of A) H* and B) N*.

3.2.3. Extended Stoltze Kinetics

As discussed in Section 4.1, the catalytic activity is observed to increase with temperature, a phenomenon attributed to the greater number of reactive sites available for catalyzing ammonia synthesis relative to the mass of the catalyst. This rise in catalytic activity corresponds to a higher site density, indicating a larger population of active sites capable of interacting with reactant molecules. Consequently, this increased site density contributes to heightened catalytic activity and enhanced efficiency in facilitating desired chemical transformations.

Contrary to the discussion in Section 4.1 regarding the influence of increasing H_2 content on ammonia efficiency, our findings, as illustrated in Figure S6, show that varying the content of N_2 in the feed gas does not lead to a significant change in ammonia efficiency. According to Stoltze's reaction mechanism for ammonia synthesis (Equations (2.1) to (2.7)), the rate-limiting step typically involves the dissociation of N_2 molecules to form adsorbed nitrogen species on the catalyst surface, necessitating the overcoming of a substantial activation energy barrier. However, once nitrogen is adsorbed, subsequent steps involving the reaction with adsorbed hydrogen species to form ammonia proceed more readily. Therefore, changes in the N_2 content of the feed gas may minimally impact the rate of ammonia synthesis, as the rate-limiting step remains unchanged.

Moreover, the active sites may exhibit a higher affinity for hydrogen species compared to nitrogen species, leading to preferential adsorption and reaction of hydrogen over nitrogen. Therefore, alterations in the N_2 content of the feed gas may not significantly affect the availability of active sites for ammonia synthesis. This preference for hydrogen adsorption on magnetite over nitrogen can be attributed to the higher energy required for nitrogen chemisorption.[19] Breaking the triple bond of N_2 necessitates overcoming a substantial energy barrier, making its adsorption less favorable compared to hydrogen. Hydrogen, with its weaker bond, can readily adsorb onto the catalyst surface with lower energy requirements, leading to its preferential adsorption and participation in the catalytic reaction steps of ammonia synthesis. Thus, it can be inferred that the site density is primarily a function of temperature and p_{H2}.

The site density for each individual experiment was calculated by minimizing $|y_{exp} - y_{model}|$. Figure S7 illustrates that for a constant N_2 partial pressure the predicted site density varies with the varying H_2:N_2 ratio and with temperature: site density decreases mostly linearly with H_2:N_2 ratio except at 548 K for high H_2:N_2 ratios, where it goes to zero. Temperature

strongly increases active site density. This strong dependency of site density on temperature and p_{N2} suggests that considering a constant value as the site density in Stoltze's kinetic model may lead to significant discrepancies between the model and experiments under various conditions.

To address this, an equation for the site density as a function of temperature and p_{H2} was obtained using the gradient descent method (as illustrated in the Supplementary Material) for the moderate active site. The training data were selected from the experiments listed in Table S2, from number 18 to 32, including all the experiments at a temperature of 598 K (9 points) and 6 points at a temperature of 648 K. Three points from the set belonging to a temperature of 648 K were excluded, as they were identified as outliers to the overall trend of site density versus H_2:N_2 ratio, as demonstrated in Figure S6 for H_2:N_2 ratios of 1.46 to 0.93. Ultimately, the equation for site density was obtained as:

$$\mu_s = 1.91(T - 618) - 1.52\left(p_{H_2} - 46.25\right) + 78.61 \quad (19)$$

Regarding the strong active site, only two data points are available at temperatures of 748 K and 773 K. These points have been excluded from this study employing the extended Stoltze kinetics due to limited data availability. To derive the site density relationship for the weak active site, the relationship between the weak and moderate active sites was first established based on the ammonia efficiency ratio of these active sites at a constant H_2:N_2 ratio. This analysis revealed a linear relationship between the two types of active sites, which was subsequently utilized to determine the site density at 548 K.

Integration of Equations (19) into (10) markedly improved the prediction of the molar fraction of ammonia, as evidenced in the parity plot (Figure 5). This enhancement was particularly evident in predicting the molar fraction of ammonia across experimental points at a constant H_2:N_2 ratio of 3.0 and temperatures ranging from 598 to 723 K, as illustrated in Figure 5. This improvement stands in contrast to the performance of both the Dyson and Simon model, as well as the Stoltze kinetic model.

The rate of ammonia synthesis, as illustrated in Figure 3, is consistent across all three temperatures as well. Notably, at 648 K, the extended Stoltze kinetics accurately captured the observed trend, even when the pH_2 reached as high as 71.27 bar, where the linear increase in ammonia synthesis rate ceases. This improvement in predictive accuracy, and the attainment of a plateau effect were consistently observed at 598 K, as illustrated in Figure 3A. Importantly, the developed kinetic model exhibited marked refinement under the challenging conditions of 548 K. By departing from the use of constant site density and instead employing an equation that varies with pH_2, the model no longer adheres to a linear relationship between ammonia synthesis rate and pH_2. Despite some overprediction at 548 K, the extended model closely approximated the observed trend. This pattern of enhancement was similarly evident in Figure 3B, where the ammonia synthesis rate was plotted against pN_2.

Evidently, the extended Stoltze kinetics exhibited enhanced predictive capability, demonstrating a closer alignment between simulated and observed data points, and deepening our understanding of the intricate relationship between temperature, pH_2, and ammonia synthesis rate. This improvement highlights the robustness and versatility of the extended Stoltze kinetics in capturing the intricate dynamics of ammonia synthesis reactions across a wide range of operating conditions. Additionally, the refined accuracy of the extended model emphasizes its potential utility in guiding experimental design and optimization strategies for industrial-scale ammonia production processes. Such advancements are crucial in addressing the challenges of sustainable ammonia synthesis and advancing our understanding of catalytic mechanisms underlying complex chemical reactions.

4. Conclusions

In this study, ammonia synthesis was investigated across a broad range of temperatures (548 K to 773 K), pressure of 90 bar, and H_2:N_2 ratios of 4:1 to 1:1, using both experimental and simulation approaches. The feasibility of employing reaction kinetic models, including the Temkin rate expression and a microkinetic model, to predict Haber-Bosch reactor performance was evaluated. Our experiments revealed intriguing trends in the synthesis of ammonia under varying conditions, illuminating the complex interplay between temperature, pressure, and reactant composition.

The experiments demonstrated that at 548 K, by increasing P_{H2} (at constant P_{N2}), the experimental molar fraction of ammonia in the outlet first increases up to P_{H2} of 28 bar and then decreases, where it reaches a plateau at $P_{H2} > 55$ bar. At 598 K, with an increase in P_{H2}, the ammonia synthesis rate increases up to the P_{H2} of 55 bar, when it peaks and then decreases. This can be explained by the hydrogen inhibition at the surface at lower temperature and high P_{H2}. Due to hydrogen adsorption's exothermic nature, hydrogen inhibition results in a further reduction in the synthesis rate at lower temperatures compared to that at higher temperatures.

The models using the Temkin-type rate expression by Dyson and Simon, as well as the microkinetic-based rate expression by Stoltze, were able to predict the experimentally synthesized ammonia satisfactorily at efficiencies between 0.15 and 0.8 and temperatures above 598 K, with the best agreement observed at 648 K for all H_2:N_2 ratios with constant N_2 or H_2 contents in the input. However, for efficiencies lower or higher than this range, an overprediction of ammonia production by the models was observed. Moreover, a remarkable discrepancy between the model predictions and the experimental mole fraction of synthesized ammonia at 548 K was observed. However, at constant hydrogen input flow but varying N_2, even though the model overpredicted ammonia production rates at 598 and 548 K, it was able to capture the trend during the increase in N_2.

The introduction of the extended Stoltze kinetics, as discussed in Section 4.2.3, marked a significant advancement in

capturing the nuanced dynamics of ammonia synthesis. By incorporating a variable site density equation dependent on temperature and p_{H2}, the extended model exhibited improved predictive accuracy across a wide range of operating conditions. Notably, the extended Stoltze kinetics accurately reproduced experimental trends, even under challenging conditions, enhancing our understanding of the intricate mechanisms governing ammonia synthesis reactions.

The enhanced precision and adaptability of the extended Stoltze kinetics open up promising pathways for guiding experimental design and optimization strategies in large-scale ammonia production processes. This model, by effectively bridging the gap between theoretical predictions and experimental observations, plays a pivotal role in advancing the development of sustainable and efficient ammonia synthesis methods. Furthermore, while the extended Stoltze kinetics has been validated against experimental data, suggesting further experiments to specifically validate this equation would reinforce the model's robustness. Such endeavors not only contribute to meeting global ammonia demands but also propel catalytic science forward by deepening our comprehension of ammonia synthesis mechanisms.

Acknowledgements

Open Access funding enabled and organized by Projekt DEAL.

Conflict of Interests

The authors declare no conflict of interest.

Data Availability Statement

The data that support the findings of this study are available in the supplementary material of this article and source data are provided with this paper in the KITopen repository under https://www.radar-service.eu/radar/de/dataset/wyd4fx4ghwfth7p0?token=IvCaySLPLIIpIsAALGNp

Keywords: Power-to-ammonia · Microkinetic model · Temkin rate expression · Industrial catalysts · Haber-Bosch process · Ammonia synthesis · Partial load

[1] C. Philibert, Ed., Renewable Energy for Industry. Paris: International Energy Agency 65, **2017**.
[2] R. Nayak-Luke, R. Bañares-Alcántara, I. Wilkinson, *Ind. Eng. Chem. Res.* **2018**, *57*(43), 14607–14616.
[3] J. Fuhrmann, M. Hülsebrock, U. Krewer, "*Energy Storage Based on Electrochemical Conversion of Ammonia*," Transition to Renewable Energy Systems, John Wiley and Sons, Ltd, **2013**, 691–706.
[4] K. Verleysen, A. Parente, F. Contino, *Energy* **2021**, *232*, 121016.
[5] I. I. Cheema, U. Krewer, *Processes* **2019**, *8*(1), 38.
[6] J. P. Vrijenhoef, "*Opportunities for Small Scale Ammonia Production*," Proceedings of the International Fertiliser Society 801, London, UK, 29th June, **2017**.
[7] E. Morgan, J. Manwell, J. McGowan, *Renew. Energy* **2014**, *72*, 51–61.
[8] S. Z. Andersen, *et al., Nature* **2019**, *570*(7762), 504–508.
[9] R. Ostuni, F. Zardi, *Method for load regulation of an ammonia plant.* US Patent No. 2013/0108538 A1, **2013**.
[10] Institute for Sustainable Process Technology (ISPT), *Power to Ammonia: feasibility study for the value chains and business cases to produce $CO 2 $-free ammonia suitable for various market applications.* **2017**.
[11] I. I. Cheema, U. Krewer, *RSC Adv.* **2018**, *8*(61), 34926–34936.
[12] G. Wang, A. Mitsos, W. Marquardt, *AIChE J.* **2020**, *66*(6), e16947.
[13] Eric R. Morgan, James F. Manwell, Jon G. McGowan, "Sustainable Ammonia Production from {U}.{S}. Offshore Wind Farms: A Techno-Economic Review," *ACS Sustain. Chem. Eng.* 5, 11, pp. 9554–9567, **2017**.
[14] A. Attari Moghaddam, U. Krewer, *Catalysts* **2020**, *10*(11), 1225.
[15] K. F. Kalz, *et al., ChemCatChem* **2017**, *9*(1), 17–29.
[16] M. Appl, "Ammonia, 2. Production Processes," *Ullmann's Encyclopedia of Industrial Chemistry*, American Cancer Society, **2011**.
[17] A. Nielsen, *An Investigation on Promoted Iron Catalysts for the Synthesis of Ammonia*, Kopenhagen: Gjellerup **1968**.
[18] M. I. Temkin, V. Pyzhev, *Acta Phys. Chim. USSR* **1940**, *12*, 327.
[19] R. Schlögl, *Angew. Chemie Int. Ed.* **2015**, *54*(11), 3465–3520.
[20] P. E. H. Nielsen, "Poisoning of Ammonia Synthesis Catalysts," *Ammonia: Catalysis and Manufacture*, (Ed: A. Nielsen) Springer, Verlag **1995**, 191–198.
[21] M. I. Temkin, N. M. Morozow, E. M. Shapatina, *Kinet. Catal* **1963**, *4*, 565.
[22] A. Cappelli, A. Collina, "Preparation of Kinetic Models for Synthesis of Ammonia on various Industrial Catalysts," in *Decision design and the computer: 117th event of the European Federation of Chemical Engineering, 5th European Symposium of the Working Party on" Routine Computer Programs and the Use of Electronic Computers in Chemical Engineering."*, no. 35, Institution of Chemical Engineers, **1972**.
[23] G. B. Ferraris, G. Donati, F. Rejna, S. Carrà, *Chem. Eng. Sci.* **1974**, *29*(7), 1621–1627.
[24] U. Guacci, F. Traina, G. B. Ferraris, R. Barisone, *Ind. Eng. Chem. Process Des. Dev.* **1977**, *16*(2), 166–176.
[25] D. C. Dyson, J. M. Simon, *Ind. Eng. Chem. Fundam.* **1968**, *7*(4), 605–610.
[26] D. Flórez-Orrego, S. de Oliveira Junior, *Energy* **2017**, *137*, 234–250.
[27] L. D. Gaines, *Chem. Eng. Sci.* **1979**, *34*(1), 37–50.
[28] P. Stoltze, *Phys. Scr.* **1987**, *36*(5), 824–864.
[29] M. Bowker, I. B. Parker, K. C. Waugh, *Appl. Catal.* **1985**, *14*, 101–118.
[30] B. Fastrup, *Top Catal* **1994**, *1*, 273–283.
[31] J. A. Dumesic, A. A. Trevino, *J. Catal.* **1989**, *116*(1), 119–129.
[32] M. Bowker, *Catal. Today* **1992**, *12*(2), 153–163.
[33] J. Sehested, C. J. H. Jacobsen, E. Törnquist, S. Rokni, P. Stoltze, *J. Catal.* **1999**, *188*(1), 83–89.
[34] J. Folke, H. Song, J. Schittkowski, R. Schlögl, H. Ruland, *Chemie Ing. Tech.* **2020**, *92*(10), 1567–1573.
[35] EUROKIN spreadsheet for assessment of transport limitations in gas-solid fixed beds https://www.eurokin.org/wp-content/uploads/webtool/EUROKIN_fixed-bed_html.htm.
[36] Z. Kowalczyk, *Catal. Lett.* **1996**, *37*, 173–179.
[37] M. Hansen, *Conshtuhon of Binary Alloys*, McGraw-Hill, New York **1958**.
[38] A. Nielsen, J. Kjaer, B. Hansen, *J. Catal.* **1964**, *3*(1), 68–79.
[39] B. Fastrup, M. Muhler, H. N. Nielsen, L. P. Nielsen, *J. Catal.* **1993**, *142*(1), 135–146.
[40] Z. Kowalczyk, J. Sentek, S. Jodzis, M. Muhler, O. Hinrichsen, *J. Catal.* **1997**, *169*(2), 407–414.

Manuscript received: May 17, 2024
Revised manuscript received: August 21, 2024
Accepted manuscript online: August 22, 2024
Version of record online: ■■, ■■

RESEARCH ARTICLE

This article investigates the performance of a Haber-Bosch reactor across a wide range of operating conditions using both Temkin and microkinetic models. Experimental validation on a magnetite-based industrial catalyst reveals critical insights into ammonia synthesis, particularly for applications in green ammonia production, where flexibility in operating conditions is essential

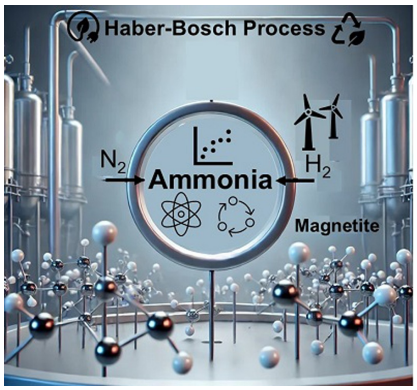

*S. Nadiri, A. Attari Moghaddam, J. Folke, H. Ruland, B. Shu, R. Fernandes, R. Schlögl, U. Krewer**